Conformational Changes and Catalytic Competency of Hydrolases Adsorbing on Fumed Silica Nanoparticles: II. Secondary Structure

Juan C. Cruz[1], Peter H. Pfromm[1]*, John M. Tomich[2], Mary E. Rezac[1]

(1) Department of Chemical Engineering, Kansas State University, 1005 Durland Hall, Manhattan, KS 66506 - 5106, USA.

(2) Department of Biochemistry and Biotechnology/Proteomics Core Facility, Kansas State University, Burt Hall, Manhattan, KS 66506 - 5106, USA.

Please cite this article in press as: J.C. Cruz et al., Conformational changes and catalytic competency of hydrolases adsorbing on fumed silica nanoparticles: II. Secondary structure, *Colloids Surf. B. Biointerfaces* (2010), doi: 10.1016/j.colsurfb.2010.06.005.

Abstract

Secondary conformational analysis via Circular Dichroism (CD) and Amide-I FTIR was applied to preparations of *Candida antarctica* Lipase B (CALB), subtilisin Carlsberg, and the Lipase from *Thermomyces lanuginosus* (TLL) on fumed silica to confirm that the "hardness" and packing density of the enzymes on the solid fumed silica nanoparticle surface can be used to rationalize the variable enzyme-dependent changes of catalytic competency with surface coverage. "Soft" enzymes should be immobilized at a surface coverage where enzyme-enzyme interactions predominate thereby preventing detrimental structural changes caused by enzyme-support interactions, while "hard" enzymes can be immobilized at low to intermediate surface coverage with good catalytic performance. Multi-layered coverage reduces the superficial average catalytic performance in all cases due to mass transfer limitations.

*Corresponding author: Tel: +1 785 532 4312; fax: +1 785 532 7372

E-mail address: pfromm@ksu.edu

Keywords: Conformational Stability; Adsorption; Fumed Silica; Protein-surface interactions; FTIR; CD.

Introduction

Use of enzymes in non-aqueous media is an alternative avenue for the production of numerous compounds of commercial interest [1-11]. The exquisite selectivity and stereoselectivity of enzymes is well recognized. Some additional advantages of enzymatic catalysis in non-aqueous media include increased solubility and stability of reactants and products [12-22], reduced complexity for downstream recovery of products and enzyme [12-22], and improved sterility [12-22]. However, enzymes are essentially insoluble in those organic solvents that do not denature them [23-26]. Various strategies have been attempted to overcome this major limitation including the incorporation of lyo- and cryo-protectants [27, 28], encapsulation in reverse micelles [29, 30], lyophilization in the presence of non-buffer salts (termed salt-activation) [7, 31], and immobilization on micro- and nano-sized organic and inorganic materials [23, 24, 26, 32, 33]. These immobilizates are often costly due in part to expensive solid supports, which ultimately limits industrial applications of non-aqueous enzymatic catalysis [34, 35].

We have immobilized enzymes on fumed silica, an inexpensive nanostructured solid support [24-26], to tackle the cost issue while maintaining or increasing catalytic efficiency. Fumed silica is a fractal aggregate with large specific surface area (up to 500 m^2/g) formed by the fusion of individual nanoparticles of approximately 10-50 nm in diameter [36-38]. Fumed silica has been successfully used for adsorbing a wide variety of compounds ranging from polymers to proteins [39-42]. Our protocol exploits these unique adsorptive properties using a two-step immobilization strategy. The enzyme molecules are first adsorbed on the nanoparticles from aqueous solution and then lyophilized to obtain the adsorbates. The lyophilized nanobiocatalysts

50 are then ready-to-use in non-aqueous media. Our protocol has been successfully applied to
51 *subtilisin Carlsberg* [25, 26] and *Candida antarctica* Lipase B (CALB) [24].

52 The maximum observed apparent catalytic activity in hexane reached or even exceeded
53 results obtained with commercial preparations of CALB, and salt-activated immobilizates for *s.*
54 *Carlsberg*. CALB is a monomeric polypeptide with 317 amino acid residues and belongs to the
55 family of globular α/β-hydrolase-like fold enzymes [43, 44]. CALB's structure contains 7
56 central β-strands flanked by 10 α-helices [43, 44]. In particular, α5 and α10 are found to be
57 extremely mobile regions that are loosely associated with the rest of the structure [45]. This
58 flexibility confers a plasticity and dynamism thought to be responsible for broadening its
59 substrate specificity [46, 47]. Four disulfide bridges help to stabilize CALB's structure [43]. The
60 *s. Carlsberg* enzyme is a single polypeptide chain enzyme with 274 amino acid residues and two
61 α/β domains that are composed of 7 central β-parallel strands flanked by 5 α-helices [48].
62 Relative to CALB, *s. Carlsberg*'s structure is more packed, which leads to a substantial
63 reduction in flexibility and dynamism.

64 The apparent catalytic activity in hexane for our enzyme/fumed silica preparations was found
65 to depend strongly on the nominal surface coverage (%SC) of the fumed silica by the enzyme
66 [24, 26]. Surprisingly, enzyme activity levels are dissimilar for *s. Carlsberg* and CALB at
67 comparable levels of surface coverage. Apparent catalytic activity increases with increasing
68 %SC at high surface coverage for both enzymes. CALB's apparent catalytic activity attains a
69 maximum at an intermediate %SC but then steeply drops with decreasing %SC. On the other
70 hand, *s. Carlsberg*'s activity remains high even at low %SC. This behavior has been explained
71 by us and others in light of three regimes of surface loading as follows: I. a low surface coverage
72 regime where enough surface area is provided for the enzyme molecules, therefore, maximizing

the opportunities for multi-point attachment and detrimental spreading. This will promote substantial conformational changes and a decrease in flexibility, which in turn leads to a reduction in activity, II. an intermediate surface coverage regime where the enzyme molecules are less dispersed thus affording beneficial interactions with neighboring molecules along with surface interactions to maintain a high population of active conformations, and III. a multi layer coverage regime where the enzyme molecules are aggregated but mass transfer limitations reduce the availability of substrate molecules to the catalytic sites.

Integrating proteins with nanomaterials has gained popularity as this approach provides an avenue for developing new materials with applications in fields as diverse as biomedicine [49-51], biosensors and bioelectronics [50, 52-55], and bioelectrochemistry [56]. One of the major challenges is to preserve protein functionality in the final biomaterial [49, 57]. This can be achieved by developing strategies to enhance the conformational stability of the adsorbed proteins [58, 59]. Numerous studies have described the crucial role of surface chemistry, size, and curvature of the nanomaterials in the conformational stability of the immobilized proteins [49, 58-63]. Recent reports have proposed that considerable attention should also be given to characterizing the different intricate surface-protein and protein-protein interactions during and after the adsorption process [61, 64, 65].

Quantifying conformational perturbations for proteins immobilized on solid supports is challenging due to the scarcity of tools for direct interrogation of the molecular rearrangements associated with structural fluctuations [66]. The most popular approaches include Fourier Transform Infrared- (FTIR), Circular Dichroism- (CD), Intrinsic Fluorescence-, Raman optical activity- and Nuclear Magnetic Resonance- (NMR) spectroscopy. CD and FTIR have been particularly useful to collect secondary structural information for both proteins in solution and

96 immobilized on solids [62, 63, 66-74]. CD spectroscopy relies on the different response of chiral
97 secondary structural components to circularly polarized light [75, 76]. Therefore, CD can be
98 successfully applied to estimate the individual contributions of α-helical, β-sheet, and less
99 ordered secondary structural components. FTIR can be also exploited for the analysis of
100 secondary structure of proteins, principally, by observing changes in the amide absorptions [67].
101 The amide group exhibits 9 vibrational modes that give rise to amide bands A, B, and I-VII [77,
102 78]. The preferred spectral components for secondary analysis are, however, amide I [79], amide
103 II [79, 80], and amide III [79, 81-83] due to the simplicity for analysis. Amide I has attracted the
104 most attention due to its increased sensitivity towards conformational changes in the secondary
105 arrangement of the protein backbone [84, 85]. This has allowed extensive use for structural
106 analyses of proteins including folding, unfolding, and aggregation [86-96]. The main challenge
107 for the analysis is posed by the overlapping of the individual structural components [97]. Two
108 strategies have been applied to overcome this issue, thereby allowing the extraction of
109 quantitative information from the spectrum: (i) resolution enhancement (also called band-
110 narrowing) [98-101] followed by curve-fitting [102, 103] and (ii) deconstruction into basis
111 spectra with a reference calibration set [104, 105]. Here we applied second derivative of the
112 amide I band as resolution enhancement method to identify the dominant secondary structural
113 components.

114 Secondary conformational stability studies of hydrolases with different native “hardness” on
115 solid fumed silica nanoparticles are performed here for both enzyme adsorbates prepared from
116 aqueous solution, and the resulting preparations after lyophilization. In both cases, the impact of
117 varying the surface coverage by the enzyme molecules was evaluated. Perturbation on the
118 intramolecular hydrogen bonding sustaining the secondary structure by attachment of the

119 enzymes to the nanoparticles was inferred from CD spectral information after normalizing with
120 respect to the native state in aqueous buffer solution. Three regions of secondary conformational
121 stability were visualized as a function of the surface coverage which correlated well with those
122 observed previously from tertiary structural analyses. The analysis confirmed also that as
123 opposed to “hard” enzymes, “soft” enzymes show a marked tendency to denature when sufficient
124 opportunities for surface interaction are provided. This can however be counteracted by
125 providing enzyme-enzyme interactions at higher levels of surface coverage. Structure modifiers
126 were added to further probe the types of interactions prevailing in each region of conformational
127 stability of immobilized enzymes. The amide I-FTIR analyses in the lyophilized state confirmed
128 alteration on the secondary structure in the low surface coverage regime and showed that
129 applying our protocol apparently does not introduce additional perturbations in the secondary
130 structure relative to those already present in the native lyophilized preparation. The FTIR
131 analysis for lyophilized preparations obtained under the crowding conditions of surface
132 coverages below 100%SC and initial enzyme concentrations above 3.0 mg/mL revealed major
133 conformational changes apparently triggered by association-induced structural transitions.
134 Emerging applications in nanobiotechnology where preserving protein conformational stability is
135 a major issue may benefit from the data discussed here [106-108].
136

Materials and Methods

Materials

Crude CALB (lyophilized; specific activity of 28U/mg solid) and TLL (lyophilized; specific activity of 1400U/mg solid) were obtained from Codexis, Inc. (Pasadena, CA), stored at 4ºC, and used as-received. TLL is a glycosylated monomeric protein with 269 amino acid residues, containing eight central β-sheets (predominantly parallel) flanked by 5 interconnecting α-helices [74, 109-111]. TLL is used for the interesterification and hydrolysis of vegetable oils and animal fats [112]. *Subtilisin Carlsberg* (EC 3.4.21.14; proteinase from *Bacillus licheniformis*; specific activity of 8 U/mg solid), fumed silica (purity of 99.8 wt.%, specific surface area 255 m^2/g, primary particle diameter ~7-50 nm, as reported by the manufacturer), ultrapure Guanidine Hydrochloride (GdmCl), 2,2,2- trifluoroethanol (TFE), and dithiothreitol (DTT) were from Sigma-Aldrich (St. Louis, MO), and used as received. Glass vials (24 mL screw-capped, flat-bottom) were used to prepare the enzyme-fumed silica suspensions.

Circular Dichroism Conditions to Monitor Unfolding

Unfolding was monitored in a cylindrical quartz cuvette (1 cm pathlength) by collecting the far-UV CD spectrum from 190 nm to 300 nm every 0.2 nm with 2 nm bandwidth and at a scan rate of 50 nm/min (Jasco J-815 spectropolarimeter, Jasco Spectroscopic Co., Hachioji, Japan, room temperature). The simple point-by-point average of three consecutive full wavelength scans is reported here. A baseline for the buffer was electronically subtracted from each enzyme spectrum (after averaging). The CD signal at 222 nm was extracted from the spectra.

Enzyme in Aqueous Buffer Solution: Unfolding by GdmCl /Urea and Unfolded Fraction Tracking by CD

When proteins undergo unfolding, the α-helical content decreases, which can be monitored by tracking the CD signal loss at 222 nm [62, 63]. The GdmCl/Urea-induced unfolding of the three hydrolases in aqueous buffer solution was normalized based on the degree of signal loss at 222 nm according to [62, 63]:

$$\phi_{GdmCl} = \left(\frac{\mathrm{CD^S}_{222} - \mathrm{CD^N}_{222}}{-\mathrm{CD^N}_{222}}\right) \qquad \textbf{Equation 1}$$

where $\boldsymbol{\phi_{GdmCl}}$ is the unfolded fraction (0, native; 1, completely unfolded).

$\mathbf{CD^S}_{\mathbf{222}}$ is the CD signal at 222 nm for enzyme molecule ensembles at any state of unfolding, and $\mathbf{CD^N}_{\mathbf{222}}$ is the CD signal at 222 nm for ensembles of native enzyme molecules both in aqueous buffer solution and in millidegrees (mdeg).

The ability of CD spectroscopy to detect unfolding was tested for reference in aqueous buffer with the powerful denaturants GdmCl and Urea. Typically, the α-helical content decreases upon exposure of the enzyme to these denaturants while both the β-sheet and random coil contents increase [72, 73], which is detected by CD due to its sensitivity to subtle changes in the secondary structure.

Crude enzyme solution was made (0.5 to 4.7 mg enzyme/mL in 10 mM monobasic phosphate buffer, adjusted to pH 7.8 by KOH 1M). GdmCl with final concentrations in the range of 1M to 6M was added followed by vortexing for about 30 seconds. Buffer solutions with final Urea concentrations from 1M to 10 M were produced and analyzed in the same manner. **Fig. 1** shows typical CD spectra for the three hydrolases in aqueous buffer solution about 30 seconds after the denaturant was added.

TLL and CALB show unfolding with increasing concentration of the denaturant (**Fig. 2**). The much more pronounced magnitude of unfolding for TLL compared to CALB at low GdmCl concentrations may be attributed to TLL's 5 α-helices vs. CALB's 10 α-helices. Thus, more denaturant is initially required per CALB molecule to promote unfolding. The modest increase in TLL's unfolding at higher GdmCl concentrations, however, could be correlated with its high conformational stability. *S. Carlsberg* shows significant resistant to unfolding (low magnitude) and a reversal of the trend at high denaturant concentrations perhaps due to the higher energy penalty associated with introducing the urea into a very rigid "hard" enzyme [113]. Similar experiments for different enzyme concentrations (not shown) confirm trends and magnitudes in **Fig. 2**.

Enzyme Adsorption: Secondary Conformational Changes of Enzymes Interacting with Fumed Silica Nanoparticles in Aqueous Buffer Solution

Secondary conformational changes of enzymes interacting with fumed silica nanoparticles were monitored by following the loss of CD signal at 222 nm. Previous studies have shown that the CD signal is not significantly scattered by the presence of nanoparticles [63, 72, 73].

CD data at 222 nm (or alternatively 235 nm for *s. Carlsberg* adsorbates at initial enzyme concentrations of 3.3 mg/mL and above, see discussion for explanation) were normalized based on the degree of signal loss according to [62, 63]:

$$\phi_{FS} = \left(\frac{\mathrm{CD_{FS}}^{\mathrm{S}}{}_{222} - \mathrm{CD}^{\mathrm{N}}{}_{222}}{-\mathrm{CD}^{\mathrm{N}}{}_{222}} \right) \qquad \textbf{Equation 2}$$

where $\boldsymbol{\phi_{FS}}$ is the average unfolded fraction for enzyme ensembles in the presence of fumed silica nanoparticles (0, native; 1, completely unfolded).

198 $\mathbf{CD_{FS}^{S}{}_{222}}$ is the net average CD signal at 222 nm of enzyme molecule ensembles interacting with
199 fumed silica at any state of unfolding in millidegrees, and $\mathbf{CD^{N}{}_{222}}$ is the average CD signal at 222
200 nm for ensembles of native enzyme molecules both in aqueous buffer and in millidegrees
201 (mdeg).

202 Crude enzymes (i.e., CALB, *s. Carlsberg* and TLL) were weighed in a glass vial and 10 mM
203 monobasic phosphate buffer (adjusted to pH 7.8 by KOH 1M) was added followed by vortexing
204 for about 30 seconds. Fumed silica was then added followed by vortexing until visually
205 homogeneous suspensions were formed (about 30 seconds) as described elsewhere [24, 26].
206 **Table 1** shows a summary of the amounts of fumed silica and enzyme used to form the
207 suspensions at the various nominal surface coverage %SC of enzyme in the final enzyme/fumed
208 silica adsorbates. The suspensions were transferred to the CD instrument for analysis.

209 *Regions of Secondary Conformational Stability: 3D Filled Contour Plots*

210 The values of unfolding tracked by changes in the CD signal at 222 nm (as a function of total
211 enzyme molecules present, compositions see **Table 1**) for each enzyme are plotted as the
212 elevation (*z*-direction) of contour plots where the *y*-axis is the concentration of enzyme in the
213 solution prior to preparing the adsorbate and the horizontal *x*-axis represents the expected %SC
214 by the enzyme molecules in the final adsorbates (**Table 1**). **Fig. 3** shows the unfolding data for
215 CALB on fumed silica as an example to introduce this type of plot. A total of 20 data points were
216 used to develop contour plots (see below). An inverse-distance algorithm (SigmaPlot®) was
217 used to interpolate. **Fig. 3** indicates that at low surface coverage unfolding becomes very
218 significant, and appears to be independent of the initial concentrations. Detailed discussions
219 follow below.

FTIR Analysis of Lyophilized Adsorbates

The adsorbates at the various %SC were placed in a refrigerator at -20°C for several hours until frozen. These preparations were then transferred to a lyophilizer where most of the water is removed by sublimation over approximately 72h as described elsewhere [24, 26]. The lyophilized powders are removed and stored at 4°C for secondary structure analysis with FTIR. Samples of approximately 0.5 mg were placed in a Spectrum 100 Fourier Transform Infrared Spectrometer (FTIR) (PerkinElmer, Waltham, MA). Absorbance IR spectra were collected from 2000 cm^{-1} to 700 cm^{-1}. The reported spectra were an average of 10 scans at 2 cm^{-1} resolution. All spectra were corrected by the automatic subtraction of water vapor and carbon dioxide using the Atmospheric Vapor Compensation (AVC) algorithm incorporated in the instrument.

Second Derivative Spectral Analysis of Lyophilized Adsorbates

The conformational state of the immobilized enzyme molecules previous to their incorporation in the reaction media was accomplished by deconstructing the information contained under the amide I region of the IR spectrum. The resolution of the original IR spectra was enhanced by taking the second derivative. This approach has been reported to narrow the half-bandwidth of the Amide I without losing the band frequencies and relative contributions of the structural components [99, 101, 114-116]. The generated peaks were then assigned to secondary structural components according to **Table 2** [67, 116-120]. The derivative was calculated with the Savitsky–Golay method (4^{th} grade polynomial, 13 smoothing points) and baseline corrected using EssentialFTIR® v.150.250.

To determine the major secondary structural components for CALB and its preparations, a sample of crude lyophilized enzyme was interrogated with the FTIR. The spectrum was collected

242 3 times and the second derivative calculated as described above. This analysis revealed that
243 1660±3 cm^{-1} and 1635±3 cm^{-1} were the dominant bands. Less intense bands were also detected at
244 1690±3 cm^{-1}, 1677±3 cm^{-1}, 1642±3 cm^{-1}, 1627±3 and 1622 ±3 cm^{-1}. The assignment to
245 secondary structural components was prepared with the reported values of **Table 2** and is
246 summarized in **Table 3**. These assignments agree well with a recent report for CALB
247 immobilized on titania [121].
248

Results and Discussion

Unfolding of Enzymes Interacting with Fumed Silica in Aqueous Solution

Fig. 4 panel A shows a comparison of the CD spectrum of native CALB in aqueous buffer solution with those of the enzyme in the presence of fumed silica nanoparticles at different levels of surface coverage (%SC). A loss of signal at 222 nm is observed with decreasing %SC and this indicates loss of the α-helical content with decreasing surface coverage. Based on secondary structure analysis with CD, Wu and Narsimhan [73] recently reported a similar loss of α-helical content when lysozyme was absorbed on 90 nm diameter *colloidal* silica nanoparticles at low surface coverages. Wu and Narsimhan [72, 73] as well as our data shown here and reported earlier [122] is also consistent with the findings of Vertegel et al. [123] for lysozyme adsorbing on 20 nm diameter *colloidal* silica nanoparticles and FRET measurements [124]. When the initial enzyme concentration in solution is increased, a substantial loss of α-helical content with respect to the native enzyme demonstrates an even higher extent of unfolding at low %SC (Panel B in **Fig. 4**). This suggests that structural perturbations leading to disruption of the hydrogen bonding network associated with the secondary structure is likely to be favored in highly crowded adsorption environments.

Similar CD experiments with *s. Carlsberg* and TLL at low enzyme concentrations (panels A of **Fig. S1** and **Fig. S2** in Supporting Information) confirm stable conformations and substantial loss of α-helical components at low %SC most likely due to increased interactions with the surface.

In summary, protein-protein interactions appear to minimize the structural perturbations that are observed at low coverage. Increased initial enzyme concentrations roughly doubled the maximum extent of unfolding of both *s. Carlsberg* and TLL (panels B of **Fig. S1** and **Fig. S2** in Supporting Information).

Regions of Secondary Conformational Stability for Enzyme/Fumed Silica Adsorbates

The secondary structure is assembled with the aid of a hydrogen bonding network along the enzyme backbone. A general view of secondary conformational stability for *s. Carlsberg* and CALB adsorbing on fumed silica was obtained by conducting multiple unfolding experiments to map secondary conformational stability of *s. Carlsberg* and CALB adsorbates on fumed silica (**Table 1)**. Conformational maps are produced (see [122] for details on this approach) to identify three regions of secondary conformational stability.

Two regions of conformational stability are observed in **Fig. 5** at surface coverages above approximately 250%SC (highly stable, region III, lighter shading) and below 250%SC (significant unfolding, region I, darker shading) with a transition (region II). Values of unfolding near unity indicate that some adsorbed enzyme molecules approach to complete denaturation. The inset in **Fig. 5** demonstrates that the catalytic competency of lyophilized adsorbates on the diagonal line in **Fig. 5** (main figure) is better at concentrations where the conformation is retained after adsorption. This also supports our hypothesis that the surface loading regimes are essentially determined during the initial adsorption step of our immobilization protocol.

As shown in **Fig. S3** in Supporting Information, three regions of secondary conformational stability were also identified for *s. Carlsberg*. When carefully examined, however, the lower section of region I (i.e., below 0.7 mg/mL) shows less unfolding compared to CALB in the same region. This could be seen as support for our hypothesis that "hard" *s. Carlsberg* has a less pronounced tendency to unfold in the presence of abundant surface area than "soft" CALB. The presence of these highly stable and functional conformations in region I is most likely responsible for the high catalytic competency in hexane of the lyophilized adsorbates in this regime (inset in **Fig. S3**, below 200%SC).

In summary, our findings confirm that the three regions of conformational stability previously identified by probing the structure at the residue scale with Trp fluorescence spectroscopy [122] are supported by CD spectroscopy. It appears, therefore, that the structural perturbations upon adsorption at low %SC are strong enough to disrupt the hydrogen bonding network responsible for stabilizing the secondary structure of the analyzed hydrolases. Additionally, the usefulness of conformational diagrams is validated here for designing coverage schemes that produced highly active and stable nanobiomaterials. Our findings also corroborate the importance of the enzyme "hardness" in defining the physical arrangement and ultimately the functionality of enzyme molecules immobilized on solid surfaces.

Impact of Structure Modifiers for Enzymes Interacting with Fumed Silica in Aqueous Buffer Solution

Structure modifying additives to the enzyme solutions were used to further investigate the intricate enzyme/fumed silica interactions.

Fig. 6 panel A demonstrates that disrupting the hydrophobic regions of CALB by addition of 30% (v/v) TFE leads to increased unfolding at higher surface coverages compared to the experiments with untreated enzymes most likely due to the higher affinity of the expose groups for the surface. At lower surface coverages, however, the flexible unfolded state of CALB molecules is likely to have a reduced molecular dynamism that leads to fewer opportunities for unfolding. This agrees with our previous data observed by following Trp fluorescence spectral shifts under the different adsorption loading schemes [122] and a recent report that suggests a positive correlation between reduced mobility on surfaces and a suppression of the tendency to spread [124].

317 Disrupting the disulfide bridges of CALB (0.5 mg/mL DTT) promotes unfolding even at lower
318 surface coverage because the exposed segments by unfolding are likely to promote a very rapid
319 and rather detrimental attachment to the abundant surface provided in this regime.
320 The impact of disrupting hydrophobic areas of *s. Carlsberg* (**Fig. 6**, panel B) shows initially
321 increased unfolding at low surface coverages most likely due to the tendency of the rigid
322 unfolded ensemble of *s. Carlsberg* to rapidly attach to the abundant surface area. At intermediate
323 surface coverages, however, the unfolding is reduced most likely due to beneficial protein-
324 protein interactions outweighing surface-protein interactions. At high surface coverages and
325 perhaps due to the association-induced conformational transitions, substantial unfolding is
326 detected. Similar trends to those described in the presence of TFE were observed for *s. Carlsberg*
327 in the presence of DTT (**Fig. 6**, panel B). This is somewhat surprising due to the absence of
328 disulfide bridges in *s. Carlsberg*'s structure. Apparently, additional interactions of DTT with the
329 secondary structure may promote intramolecular instabilities that may lead to the disruption of
330 the hydrogen bonding network and ultimately to unfolding. This behavior was not detected
331 previously in the Trp fluorescence spectroscopy studies [122].

332 *Secondary Conformational Changes for Lyophilized Adsorbates*

333 **Fig. 7** shows that the FT-infrared absorbance increases with increasing surface coverage
334 towards the absorbance of native lyophilized CALB with no silica present. Because the silica
335 does not absorb in this region of the spectrum, the observed FTIR signal emerges only from the
336 enzyme and corroborates an increasingly higher surface packing density with increasing surface
337 coverage.
338 The position and number of the secondary structural components for the preparations obtained
339 at 2%SC and 1250%SC are shown in **Fig. 8** panel A and B, respectively. These components

were determined with the second derivative and assigned according to **Table 3**. The 1250%SC lyophilized preparation clearly shows two dominant bands at 1636.4 cm^{-1} and 1656.8 cm^{-1}. These two bands can be attributed to the β-sheets and α-helices, respectively, representing aspects of CALB's native conformation [121]. This support the notion that at high %SC attachment to the nanoparticles in single or perhaps multiple layers does not alter the secondary structure significantly. The 2%SC preparation, however, has a dominant broad band that peaks at 1645.1 cm^{-1}. This band has been ascribed to disordered components most likely resulting from rearrangements within the enzyme secondary structure as expected upon spreading on the surface. Bands at 1672.4 cm^{-1} and at 1628.1 cm^{-1} can be ascribed to turns and β-sheets, respectively, which are also present when significant rearrangements occur in the secondary structure [121].

In summary, the amide I-FTIR analysis confirms the substantial loss of α-helical content relative to the native state that was detected with CD for adsorbates obtained at low %SC, and supports the idea of very well maintained structures at high %SC.

Prevention of conformational changes to maintain catalytic competency is clearly an important issue. It has been suggested that increasing the enzyme concentration in the aqueous phase during immobilization would be beneficial to reduce detrimental conformational changes [125]. The results from CD and fluorescence spectroscopy suggest that at low %SC this approach leads to substantial conformational changes in both the secondary (upper part of region I in **Fig. 5** and **Fig. S3**, darker areas) and tertiary structure. This approach is therefore tested below for the 17%SC preparation obtained at different initial enzyme concentrations.

Adsorbates with 17%SC were obtained from enzyme solutions with initial concentrations ranging from 0.3 mg/mL to 4.7 mg/mL. The adsorbates were then lyophilized and the amide I

363 FTIR spectra collected (data not shown). The occurrence of secondary structure conformational
364 changes was examined further via FTIR spectra and the second derivative of these spectra for the
365 preparations obtained from 0.3 and 4.7 mg enzyme/mL solution, **Fig. 9** panels A and B,
366 respectively. Band assignments were according to **Table 3**.

367 As shown in **Fig. 9** panel A, two dominant bands that peak at 1660.5 cm^{-1} and 1649.0 cm^{-1}
368 were detected for the 0.3 mg/mL case, which can be assigned to α-helix and disordered
369 components, respectively. Less intense signals were detected at 1673.5 cm^{-1} and 1627.7 cm^{-1},
370 that are normally attributed to turns and β-sheets. This suggests partially folded structures since
371 the α-helical ordered components are still relatively abundant.

372 **Fig. 9** panel B shows the second derivative for the 4.7 mg enzyme/mL case. A substantial loss
373 of signal at 1660.0 cm^{-1} was detected relative to that observed at low concentration. This can be
374 explained by a significant decrease in the α-helical content. The contribution of disordered
375 components (1644.0 cm^{-1}), turns (1673.5 cm^{-1}), β-aggregates (1626.5 cm^{-1}), and β-sheets (1635.5
376 cm^{-1}) significantly increased. Similar results were obtained for 2 and 10 %SC preparations (data
377 not shown). This suggests that obtaining adsorbates under crowding conditions and especially in
378 the region of low %SC should be avoided as it may lead to considerable unfolding.

379 Similar studies for lyophilized preparations have identified a loss of α-helical components
380 concomitantly with an increase in the β-sheet, turns, and disordered components and suggested
381 association-induced conformational transitions occurring either pre- or post- immobilization as a
382 possible trigger mechanism [126-129].

383

Conclusions

We have confirmed that the existence of three regions of conformational stability for hydrolases adsorbing on fumed silica as a function of the nominal surface coverage (%SC) can be seen at the secondary structural level upon disruption of the well organized intramolecular hydrogen bonding network of these enzyme molecules. Unfolding data was inferred from far-UV CD spectra of adsorbing hydrolases on fumed silica. At low %SC, enzyme molecules were seen to undergo major conformational changes. This region of low conformational stability is thought to occur due to increased interactions of the enzyme molecules with excess silica surface area. This phenomenon was exacerbated for CALB, which is an enzyme with a loosely packed or "soft" structure. The loss in catalytic activity in hexane for fumed silica based CALB nanobiocatalysts prepared in this region can be, therefore, correlated with this surface-induced structural distortion as it may ultimately lead to disruption of the active site. The "hard" *s. Carlsberg* enzyme at low %SC showed a relatively higher tolerance to surface-induced unfolding, which appeared to correlate well with the high activity in hexane of lyophilized adsorbates at low %SC. At an intermediate %SC of about 250%, a region of transitional stability was identified where enzyme molecules have stable conformations and clustering appears to be absent. This region appears to be correlated with an optimum in catalytic activity for CALB in hexane. At high %SC, enzyme structure is well maintained which could be attributed to a different energy landscape where strong interactions with the surface are suppressed and protein-protein interactions dominate. This region is characterized by enzyme multilayer packing on the surface, which resulted in a substantial loss of catalytic activity of nanobiocatalysts in hexane due principally to mass transfer limitations.

406 TFE (30% v/v) incubation revealed the importance of hydrophobic segments in maintaining
407 the CALB's structure at high %SC. At low %SC, however, this approach seemed to support the
408 idea that suppression of protein dynamics could be a useful strategy to avoid spreading on
409 surfaces. The static structure of *s. Carlsberg* is postulated to be responsible for the even higher
410 levels of unfolding in the presence of TFE at low %SC. DTT addition increased the unfolding
411 levels of CALB for all %SC cases, which suggested that the exposed regions had increased
412 affinity for the surface as well as poor mobility.
413 Amide-I FTIR secondary analysis for CALB lyophilized adsorbates with low %SC showed a
414 marked decrease in the α-helical component signal. This further supported the notion of induced
415 structural perturbation when sufficient surface area is provided for immobilization. Filled
416 contour conformational maps suggested that an increase in the initial enzyme concentration at
417 low %SC gives rise to a pronounced unfolding most likely due to association-induced
418 conformational transitions. The FTIR analysis corroborated that for the lyophilized adsorbates of
419 CALB with low %SC, turns and β-sheets dominated over α-helical components.
420

References

[1] M.N. Gupta, Enzyme Function in Organic-Solvents, Eur. J. Biochem., 203 (1992) 25-32.

[2] H. Kise, Ester and Peptide-Synthesis by Proteases in Organic-Solvents, Journal of Synthetic Organic Chemistry Japan, 49 (1991) 42-51.

[3] A.M. Klibanov, Improving enzymes by using them in organic solvents, Nature, 409 (2001) 241-246.

[4] A.M. Klibanov, Asymmetric enzymatic oxidoreductions in organic solvents, Curr. Opin. Biotechnol., 14 (2003) 427-431.

[5] J.O. Rich and Y.L. Khmelnitsky, Phospholipase D-catalyzed transphosphatidylation in anhydrous organic solvents, Biotechnol. Bioeng., 72 (2001) 374-377.

[6] M.T. Ru, S.Y. Hirokane, A.S. Lo, J.S. Dordick, J.A. Reimer and D.S. Clark, On the salt-induced activation of lyophilized enzymes in organic solvents: Effect of salt kosmotropicity on enzyme activity, J. Am. Chem. Soc., 122 (2000) 1565-1571.

[7] M.T. Ru, K.C. Wu, J.P. Lindsay, J.S. Dordick, J.A. Reimer and D.S. Clark, Towards more active biocatalysts in organic media: Increasing the activity of salt-activated enzymes, Biotechnol. Bioeng., 75 (2001) 187-196.

[8] A. Zaks and A.J. Russell, Enzymes in Organic-Solvents - Properties and Applications, J. Biotechnol., 8 (1988) 259-270.

[9] D.S. Clark, Characteristics of nearly dry enzymes in organic solvents: implications for biocatalysis in the absence of water, Philos. Trans. R. Soc. Lond. Ser. B-Biol. Sci., 359 (2004) 1299-1307.

[10] S. Kamat, J. Barrera, E.J. Beckman and A.J. Russell, Biocatalytic Synthesis of Acrylates in Organic-Solvents and Supercritical Fluids .1. Optimization of Enzyme Environment, Biotechnol. Bioeng., 40 (1992) 158-166.

[11] A. Gupta and S.K. Khare, Enzymes from solvent-tolerant microbes: Useful biocatalysts for non-aqueous enzymology, Crit. Rev. Biotechnol., 29 (2009) 44-54.

[12] A. Ghanem, Trends in lipase-catalyzed asymmetric access to enantiomerically pure/enriched compounds, Tetrahedron, 63 (2007) 1721-1754.

[13] A. Ghanem and H.Y. Aboul-Enein, Application of lipases in kinetic resolution of racemates, Chirality, 17 (2005) 1-15.

[14] G. Carrea and S. Riva, Properties and synthetic applications of enzymes in organic solvents, Angew. Chem., Int. Edit., 39 (2000) 2226-2254.

[15] J.S. Dordick, Designing Enzymes for Use in Organic-Solvents, Biotechnol. Prog., 8 (1992) 259-267.

[16] J.S. Dordick, Y.L. Khmelnitsky and M.V. Sergeeva, The evolution of biotransformation technologies, Curr. Opin. Biotechnol., 1 (1998) 311-318.

[17] J.A. Akkara, M.S.R. Ayyagari and F.F. Bruno, Enzymatic synthesis and modification of polymers in nonaqueous solvents, Trends Biotechnol., 17 (1999) 67-73.

[18] Y.L. Khmelnitsky and J.O. Rich, Biocatalysis in nonaqueous solvents, Curr. Opin. Chem. Biol., 3 (1999) 47-53.

[19] P.J. Halling, Biocatalysis in low-water media: understanding effects of reaction conditions, Curr. Opin. Chem. Biol., 4 (2000) 74-80.

[20] H. Ogino and H. Ishikawa, Enzymes which are stable in the presence of organic solvents, J. Biosci. Bioeng., 91 (2001) 109-116.

[21] G.R. Castro and T. Knubovets, Homogeneous biocatalysis in organic solvents and water-organic mixtures, Crit. Rev. Biotechnol., 23 (2003) 195-231.
[22] A.L. Serdakowski and J.S. Dordick, Enzyme activation for organic solvents made easy, Trends Biotechnol., 26 (2008) 48-54.
[23] M. Persson, E. Wehtje and P. Adlercreutz, Factors governing the activity of lyophilised and immobilised lipase preparations in organic solvents, ChemBioChem, 3 (2002) 566-571.
[24] J.C. Cruz, P.H. Pfromm and M.E. Rezac, Immobilization of Candida antarctica Lipase B on fumed silica, Process Biochem., 44 (2009) 62-69.
[25] P.H. Pfromm, M.E. Rezac, K. Wurges and P. Czermak, Fumed silica activated subtilisin Carlsberg in hexane in a packed-bed reactor, AIChE J., 53 (2007) 237-242.
[26] K. Wurges, P.H. Pfromm, M.E. Rezac and P. Czermak, Activation of subtilisin Carlsberg in hexane by lyophilization in the presence of fumed silica, J. Mol. Catal. B: Enzym., 34 (2005) 18-24.
[27] K. Dabulis and A.M. Klibanov, Dramatic Enhacement of Enzymatic-Aactivity in Organic-Solvents by Lyoprotectants, Biotechnol. Bioeng., 41 (1993) 566-571.
[28] A.O. Triantafyllou, E. Wehtje, P. Adlercreutz and B. Mattiasson, How do additives affect enzyme activity and stability in nonaqueous media?, Biotechnol. Bioeng., 54 (1997) 67-76.
[29] C.M.L. Carvalho and J.M.S. Cabral, Reverse micelles as reaction media for lipases, Biochimie, 82 (2000) 1063-1085.
[30] M.A. Biasutti, E.B. Abuin, J.J. Silber, N.M. Correa and E.A. Lissi, Kinetics of reactions catalyzed by enzymes in solutions of surfactants, Adv. Colloid Interface Sci., 136 (2008) 1-24.
[31] J.P. Lindsay, D.S. Clark and J.S. Dordick, Penicillin amidase is activated for use in nonaqueous media by lyophilizing in the presence of potassium chloride, Enzyme Microb. Technol., 31 (2002) 193-197.
[32] A.X. Yan, X.W. Li and Y.H. Ye, Recent progress on immobilization of enzymes on molecular sieves for reactions in organic solvents, Appl. Biochem. Biotechnol., 101 (2002) 113-129.
[33] B. Chen, J. Hu, E.M. Miller, W.C. Xie, M.M. Cai and R.A. Gross, Candida antarctica lipase B chemically immobilized on epoxy-activated micro- and nanobeads: Catalysts for polyester synthesis, Biomacromolecules, 9 (2008) 463-471.
[34] B. Chen, E.M. Miller, L. Miller, J.J. Maikner and R.A. Gross, Effects of macroporous resin size on Candida antarctica lipase B adsorption, fraction of active molecules, and catalytic activity for polyester synthesis, Langmuir, 23 (2007) 1381-1387.
[35] B. Chen, M.E. Miller and R.A. Gross, Effects of porous polystyrene resin parameters on Candida antarctica Lipase B adsorption, distribution, and polyester synthesis activity, Langmuir, 23 (2007) 6467-6474.
[36] V.M. Gun'ko, I.F. Mironyuk, V.I. Zarko, V.V. Turov, E.F. Voronin, E.M. Pakhlov, E.V. Goncharuk, R. Leboda, J. Skubiszewska-Zieba, W. Janusz, S. Chibowski, Y.N. Levchuk and A.V. Klyueva, Fumed silicas possessing different morphology and hydrophilicity, J. Colloid Interface Sci., 242 (2001) 90-103.
[37] V.M. Gun'ko, I.F. Mironyuk, V.I. Zarko, E.F. Voronin, V.V. Turov, E.M. Pakhlov, E.V. Goncharuk, Y.M. Nychiporuk, N.N. Vlasova, P.P. Gorbik, O.A. Mishchuk, O.A. Mishchuk, A.A. Chuiko, T.V. Kulik, B.B. Palyanytsya, S.V. Pakhovchishin, J. Skubiszewska-Zieba, W. Janusz, A.V. Turov and R. Leboda, Morphology and surface properties of fumed silicas, J. Colloid Interface Sci., 289 (2005) 427-445.
[38] R.K. Iler, The Chemistry of Silica, John Wiley & Sons, Inc., 1979.

[39] V.M. Gun'ko, I.V. Mikhailova, V.I. Zarko, Gerashchenko, II, N.V. Guzenko, W. Janusz, R. Leboda and S. Chibowski, Study of interaction of proteins with fumed silica in aqueous suspensions by adsorption and photon correlation spectroscopy methods, J. Colloid Interface Sci., 260 (2003) 56-69.
[40] V.M. Gun'ko, E.F. Voronin, L.V. Nosach, E.M. Pakhlov, N.V. Guzenko, R. Leboda and J. Skubiszewska-Zieba, Adsorption and migration of poly(vinyl pyrrolidone) at a fumed silica surface, Adsorpt. Sci. Technol., 24 (2006) 143-157.
[41] V.M. Gun'ko, V.I. Zarko, E.F. Voronin, E.V. Goncharuk, L.S. Andriyko, N.V. Guzenko, L.V. Nosach and W. Janusz, Successive interaction of pairs of soluble organics with nanosilica in aqueous media, J. Colloid Interface Sci., 300 (2006) 20-32.
[42] V.M. Gun'ko, V.I. Zarko, E.F. Voronin, V.V. Turov, I.F. Mironyuk, Gerashchenko, II, E.V. Goncharuk, E.M. Pakhlov, N.V. Guzenko, R. Leboda, J. Skubiszewska-Zieba, W. Janusz, S. Chibowski, Y.N. Levchuk and A.V. Klyueva, Impact of some organics on structural and adsorptive characteristics of fumed silica in different media, Langmuir, 18 (2002) 581-596.
[43] J. Uppenberg, M.T. Hansen, S. Patkar and T.A. Jones, Sequence, Crystal-Structure Determination and Refinement of 2 Crystal Forms of Lipase-B From *Candida antarctica*, Structure, 2 (1994) 293-308.
[44] J. Uppenberg, N. Ohrner, M. Norin, K. Hult, G.J. Kleywegt, S. Patkar, V. Waagen, T. Anthonsen and T.A. Jones, Crystallographic and molecular-modeling studies of lipase B from Candida antarctica reveal a stereospecificity pocket for secondary alcohols, Biochemistry, 34 (1995) 16838-16851.
[45] M. Skjot, L. De Maria, R. Chatterjee, A. Svendsen, S.A. Patkar, P.R. Ostergaard and J. Brask, Understanding the Plasticity of the alpha/beta Hydrolase Fold: Lid Swapping on the Candida antarctica Lipase B Results in Chimeras with Interesting Biocatalytic Properties, ChemBioChem, 10 (2009) 520-527.
[46] K. Hult and P. Berglund, Enzyme promiscuity: mechanism and applications, Trends Biotechnol., 25 (2007) 231-238.
[47] M. Svedendahl, P. Carlqvist, C. Branneby, O. Allner, A. Frise, K. Hult, P. Berglund and T. Brinck, Direct Epoxidation in Candida antarctica Lipase B Studied by Experiment and Theory, ChemBioChem, 9 (2008) 2443-2451.
[48] D.J. Neidhart and G.A. Petsko, The Refined Crystal-Structure of Subtilisin Carlsberg at 2.5 A Resolution, Protein Engineering, 2 (1988) 271-276.
[49] P. Asuri, S.S. Bale, S.S. Karajanagi and R.S. Kane, The protein-nanomaterial interface, Curr. Opin. Biotechnol., 17 (2006) 562-568.
[50] N.A. Kotov, J.O. Winter, I.P. Clements, E. Jan, B.P. Timko, S. Campidelli, S. Pathak, A. Mazzatenta, C.M. Lieber, M. Prato, R.V. Bellamkonda, G.A. Silva, N.W.S. Kam, F. Patolsky and L. Ballerini, Nanomaterials for Neural Interfaces, Adv. Mater., 21 (2009) 3970-4004.
[51] X. Wang, L.H. Liu, O. Ramstrom and M.D. Yan, Engineering Nanomaterial Surfaces for Biomedical Applications, Exp. Biol. Med., 234 (2009) 1128-1139.
[52] A. Noy, A.B. Artyukhin and N. Misra, Bionanoelectronics with 1D materials, Mater. Today, 12 (2009) 22-31.
[53] E. Katz and I. Willner, Biomolecule-functionalized carbon nanotubes: Applications in nanobioelectronics, Chemphyschem, 5 (2004) 1085-1104.
[54] A.K. Sarma, P. Vatsyayan, P. Goswami and S.D. Minteer, Recent advances in material science for developing enzyme electrodes, Biosens. Bioelectron., 24 (2009) 2313-2322.

[55] L.J. Mi, X. Zhang, W.C. Yang, L.H. Wang, Q. Huang, C.H. Fan and J. Hu, Artificial Nano-Bio-Complexes: Effects of Nanomaterials on Biomolecular Reactions and Applications in Biosensing and Detection, J. Nanosci. Nanotechnol., 9 (2009) 2247-2255.
[56] D. Chen, G. Wang and J.H. Li, Interfacial bioelectrochemistry: Fabrication, properties and applications of functional nanostructured biointerfaces, J. Phys. Chem. C, 111 (2007) 2351-2367.
[57] R.S. Kane and A.D. Stroock, Nanobiotechnology: Protein-nanomaterial interactions, Biotechnol. Prog., 23 (2007) 316-319.
[58] P. Asuri, S.S. Karajanagi, A.A. Vertegel, J.S. Dordick and R.S. Kane, Enhanced stability of enzymes adsorbed onto nanoparticles, J. Nanosci. Nanotechnol., 7 (2007) 1675-1678.
[59] P. Asuri, S.S. Karajanagi, H.C. Yang, T.J. Yim, R.S. Kane and J.S. Dordick, Increasing protein stability through control of the nanoscale environment, Langmuir, 22 (2006) 5833-5836.
[60] P. Asuri, S.S. Bale, R.C. Pangule, D.A. Shah, R.S. Kane and J.S. Dordick, Structure, function, and stability of enzymes covalently attached to single-walled carbon nanotubes, Langmuir, 23 (2007) 12318-12321.
[61] N. Shamim, H. Liang, K. Hidajat and M.S. Uddin, Adsorption, desorption, and conformational changes of lysozyme from thermosensitive nanomagnetic particles, J. Colloid Interface Sci., 320 (2008) 15-21.
[62] W. Shang, J.H. Nuffer, J.S. Dordick and R.W. Siegel, Unfolding of ribonuclease A on silica nanoparticle surfaces, Nano Lett., 7 (2007) 1991-1995.
[63] W. Shang, J.H. Nuffer, V.A. Muniz-Papandrea, W. Colon, R.W. Siegel and J.S. Dordick, Cytochrome c on Silica Nanoparticles: Influence of Nanoparticle Size on Protein Structure, Stability, and Activity, Small, 5 (2009) 470-476.
[64] W. Norde, Driving forces for protein adsorption at solid surfaces, in: Biopolymers at Interfaces, Marcel Dekker, Inc., New York, 2003.
[65] P. Roach, D. Farrar and C.C. Perry, Surface tailoring for controlled protein adsorption: Effect of topography at the nanometer scale and chemistry, J. Am. Chem. Soc., 128 (2006) 3939-3945.
[66] A. Ganesan, B.D. Moore, S.M. Kelly, N.C. Price, O.J. Rolinski, D.J.S. Birch, I.R. Dunkin and P.J. Halling, Optical Spectroscopic Methods for Probing the Conformational Stability of Immobilised Enzymes, Chemphyschem, 10 (2009) 1492-1499.
[67] A. Barth, Infrared spectroscopy of proteins, Biochim. Biophys. Acta, Bioenerg., 1767 (2007) 1073-1101.
[68] A. Ganesan, N.C. Price, S.M. Kelly, I. Petry, B.D. Moore and P.J. Halling, Circular dichroism studies of subtilisin Carlsberg immobilised on micron sized silica particles, Biochim. Biophys. Acta, Proteins Proteomics, 1764 (2006) 1119-1125.
[69] K. Hidajat, M. Uddin and Z. Peng, Conformational change of adsorbed and desorbed bovine serum albumin on nano-sized magnetic particles, Colloids Surf., B, 33 (2004) 15-21.
[70] A. Kondo, S. Oku and K. Higashitani, Structural-Changes in Protein Molecules Adsorbed on Ultrafine Silica Particles, J. Colloid Interface Sci., 143 (1991) 214-221.
[71] R. Pribic, I.H.M. Vanstokkum, D. Chapman, P.I. Haris and M. Bloemendal, Protein Secondary Structure from Fourier-Transform Infrares and/or Circular-Dichroism Spectra, Anal. Biochem., 214 (1993) 366-378.
[72] X. Wu and G. Narsimhan, Characterization of secondary and tertiary conformational changes of beta-lactoglobulin adsorbed on silica nanoparticle surfaces, Langmuir, 24 (2008) 4989-4998.

601 [73] X.Y. Wu and G. Narsimhan, Effect of surface concentration on secondary and tertiary
602 conformational changes of lysozyme adsorbed on silica nanoparticles, Biochim. Biophys. Acta,
603 Proteins Proteomics, 1784 (2008) 1694-1701.
604 [74] K. Zhu, A. Jutila, E.K.J. Tuominen, S.A. Patkar, A. Svendsen and P.K.J. Kinnunen, Impact
605 of the tryptophan residues of Humicola lanuginosa lipase on its thermal stability, Biochim.
606 Biophys. Acta, Protein Struct. Molec. Enzym., 1547 (2001) 329-338.
607 [75] S.M. Kelly, T.J. Jess and N.C. Price, How to study proteins by circular dichroism, Biochim.
608 Biophys. Acta, Proteins Proteomics, 1751 (2005) 119-139.
609 [76] B. Ranjbar and P. Gill, Circular Dichroism Techniques: Biomolecular and Nanostructural
610 Analyses- A Review, Chem. Biol. Drug Des., 74 (2009) 101-120.
611 [77] J. Bandekar, Amide Modes and Protein Conformation, Biochim. Biophys. Acta, 1120
612 (1992) 123-143.
613 [78] S. Krimm and J. Bandekar, Vibrational Spectroscopy and Conformation of Peptides,
614 Polypeptides, and Proteins, Adv. Protein Chem., 38 (1986) 181-364.
615 [79] J.L.R. Arrondo, A. Muga, J. Castresana and F.M. Goni, Quantitative Studies of the
616 Structure of Proteins in Solution by Fourier-Transform Infrared-Spectroscopy, Prog. Biophys.
617 Mol. Biol., 59 (1993) 23-56.
618 [80] K.A. Oberg, J.M. Ruysschaert and E. Goormaghtigh, The optimization of protein secondary
619 structure determination with infrared and circular dichroism spectra, Eur. J. Biochem., 271
620 (2004) 2937-2948.
621 [81] F.N. Fu, D.B. Deoliveira, W.R. Trumble, H.K. Sarkar and B.R. Singh, Secondary Structure
622 Estimation of Proteins Using the Amide-III Region of Fourier-Transform Infrared-Spectroscopy
623 - Application to Analyze Calcium Binding-Induced Structural-Changes in Calsequestrin, Appl.
624 Spectrosc., 48 (1994) 1432-1441.
625 [82] S.W. Cai and B.R. Singh, A distinct utility of the amide III infrared band for secondary
626 structure estimation of aqueous protein solutions using partial least squares methods,
627 Biochemistry, 43 (2004) 2541-2549.
628 [83] S.W. Cai and B.R. Singh, Identification of beta-turn and random coil amide III infrared
629 bands for secondary structure estimation of proteins, Biophys. Chem., 80 (1999) 7-20.
630 [84] Y.N. Chirgadze and N.A. Nevskaya, Infrared-Spectra and Resonance Interaction of Amide-
631 I Vibration of Anti-Parallel-Chain Pleated Sheet, Biopolymers, 15 (1976) 607-625.
632 [85] Y.N. Chirgadze and N.A. Nevskaya, Infrared-Spectra and Resonance Interaction of Amide-
633 I Vibration of Parallel-Chain Pleated Sheet, Biopolymers, 15 (1976) 627-636.
634 [86] E. Kauffmann, N.C. Darnton, R.H. Austin, C. Batt and K. Gerwert, Lifetimes of
635 intermediates in the beta-sheet to alpha-helix transition of beta-lactoglobulin by using a
636 diffusional IR mixer, Proc. Natl. Acad. Sci. U. S. A., 98 (2001) 6646-6649.
637 [87] H. Fabian, H.H. Mantsch and C.P. Schultz, Two-dimensional IR correlation spectroscopy:
638 Sequential events in the unfolding process of the lambda Cro-V55C repressor protein, Proc. Natl.
639 Acad. Sci. U. S. A., 96 (1999) 13153-13158.
640 [88] D. Reinstadler, H. Fabian and D. Naumann, New structural insights into the refolding of
641 ribonuclease T1 as seen by time-resolved Fourier-transform infrared spectroscopy, Proteins-
642 Structure Function and Genetics, 34 (1999) 303-316.
643 [89] R.B. Dyer, F. Gai and W.H. Woodruff, Infrared studies of fast events in protein folding,
644 Acc. Chem. Res., 31 (1998) 709-716.

645 [90] A.P. Ramajo, S.A. Petty, A. Starzyk, S.M. Decatur and M. Volk, The alpha-helix folds
646 more rapidly at the C-terminus than at the N-terminus, J. Am. Chem. Soc., 127 (2005) 13784-
647 13785.
648 [91] J. Backmann, H. Fabian and D. Naumann, Temperature-Jump-Induced Refolding of
649 Ribonuclease-A - A Time-Resolved FTIR Spectroscopic Study, FEBS Lett., 364 (1995) 175-
650 178.
651 [92] W.K. Surewicz, A.G. Szabo and H.H. Mantsch, Conformational Properties of Azurin in
652 Solution as Determined from Resolution-Enhanced Fourier-Transform Infrared-Spectra, Eur. J.
653 Biochem., 167 (1987) 519-523.
654 [93] D. Reinstadler, H. Fabian, J. Backmann and D. Naumann, Refolding of thermally and urea-
655 denatured ribonuclease A monitored by time-resolved FTIR spectroscopy, Biochemistry, 35
656 (1996) 15822-15830.
657 [94] H. Fabian and D. Naumann, Methods to study protein folding by stopped-flow FT-IR,
658 Methods, 34 (2004) 28-40.
659 [95] E.A. Gooding, A.P. Ramajo, J.W. Wang, C. Palmer, E. Fouts and M. Volk, The effects of
660 individual amino acids on the fast folding dynamics of alpha-helical peptides, Chem. Commun.,
661 (2005) 5985-5987.
662 [96] S.H. Brewer, B.B. Song, D.P. Raleigh and R.B. Dyer, Residue specific resolution of protein
663 folding dynamics using isotope-edited infrared temperature jump spectroscopy, Biochemistry, 46
664 (2007) 3279-3285.
665 [97] J.K. Kauppinen, D.J. Moffatt, H.H. Mantsch and D.G. Cameron, Fourier Self-
666 Deconvolution - A Method for Resolving Intrinsically Overlapped Bands, Appl. Spectrosc., 35
667 (1981) 271-276.
668 [98] H.H. Mantsch, D.J. Moffatt and H.L. Casal, Fourier-Transform Methods for Spectral
669 Resolution Enhancement, J. Mol. Struct., 173 (1988) 285-298.
670 [99] H. Susi and D.M. Byler, Resolution-Enhanced Fourier-Transform Infrared-Spectroscopy of
671 Enzymes, Method Enzymol., 130 (1986) 290-311.
672 [100] A. Barth, Fine-structure enhancement - assessment of a simple method to resolve
673 overlapping bands in spectra, Spectroc. Acta Pt. A, Molec. Biomolec. Spectr., 56 (2000) 1223-
674 1232.
675 [101] A. Dong, P. Huang and W.S. Caughey, Redox-Dependent Changes in Beta-Extended
676 Chain and Turn Structures of Cytochrome-C in Water Solution Determined by 2nd Derivative
677 Amide-I Infrared-Spectra, Biochemistry, 31 (1992) 182-189.
678 [102] H. Susi and D.M. Byler, Fourier-Transform Infrared Study of Proteins with Parallel Beta-
679 Chains, Arch. Biochem. Biophys., 258 (1987) 465-469.
680 [103] D.M. Byler and H. Susi, Examination of the Secondary Structure of Proteins by
681 Deconvolved FTIR Spectra, Biopolymers, 25 (1986) 469-487.
682 [104] R.W. Sarver and W.C. Krueger, Protein Secondary Structure from Fourier-Transform
683 Infrared-Spectroscopy - A Data-Base Analysis, Anal. Biochem., 194 (1991) 89-100.
684 [105] V. Baumruk, P. Pancoska and T.A. Keiderling, Predictions of secondary structure using
685 statistical analyses of electronic and vibrational circular dichroism and Fourier transform infrared
686 spectra of proteins in H_2O, J. Mol. Biol., 259 (1996) 774-791.
687 [106] J. Wang, Nanomaterial-based electrochemical biosensors, Analyst, 130 (2005) 421-426.
688 [107] J.L. West and N.J. Halas, Engineered nanomaterials for biophotonics applications:
689 Improving sensing, imaging, and therapeutics, Annu. Rev. Biomed. Eng., 5 (2003) 285-292.

690 [108] J.J. Gray, The interaction of proteins with solid surfaces, Curr. Opin. Struct. Biol., 14
691 (2004) 110-115.
692 [109] A. Jutila, K. Zhu, S.A. Patkar, J. Vind, A. Svendsen and P.K.J. Kinnunen, Detergent-
693 induced conformational changes of Humicola lanuginosa lipase studied by fluorescence
694 spectroscopy, Biophys. J., 78 (2000) 1634-1642.
695 [110] A. Jutila, K. Zhu, E.K.J. Tuominen and P.K.J. Kinnunen, Fluorescence spectroscopic
696 characterization of Humicola lanuginosa lipase dissolved in its substrate, Biochim. Biophys.
697 Acta, Proteins Proteomics, 1702 (2004) 181-189.
698 [111] K. Zhu, A. Jutila and P.K.J. Kinnunen, Steady state and time resolved effects of guanidine
699 hydrochloride on the structure of Humicola lanuginosa lipase revealed by fluorescence
700 spectroscopy, Protein Sci., 9 (2000) 598-609.
701 [112] T. Schafer, T.W. Borchert, V.S. Nielsen, P. Skagerlind, K. Gibson, K. Wenger, F. Hatzack,
702 L.D. Nilsson, S. Salmons, S. Pedersen, H.P. Heldt-Hansen, P.B. Poulsen, H. Lund, K.M.
703 Oxenboll, G.F. Wu, H.H. Pedersen and H. Xu, Industrial enzymes, in: White Biotechnology,
704 Vol 105, Springer-Verlag Berlin, Berlin, 2007, pp. 59-131.
705 [113] F. Guo and J.M. Friedman, Osmolyte-Induced Perturbations of Hydrogen Bonding
706 between Hydration Layer Waters: Correlation with Protein Conformational Changes, J. Phys.
707 Chem. B, 113 (2009) 16632-16642.
708 [114] S.F. Bai and A.C. Dong, Effects of immobilization onto aluminum hydroxide particles on
709 the thermally induced conformational behavior of three model proteins, Int. J. Biol. Macromol.,
710 45 (2009) 80-85.
711 [115] A.C. Dong, L.S. Jones, B.A. Kerwin, S. Krishnan and J.F. Carpenter, Secondary structures
712 of proteins adsorbed onto aluminum hydroxide: Infrared spectroscopic analysis of proteins from
713 low solution concentrations, Anal. Biochem., 351 (2006) 282-289.
714 [116] A. Natalello, D. Ami, S. Brocca, M. Lotti and S.M. Doglia, Secondary structure,
715 conformational stability and glycosylation of a recombinant Candida rugosa lipase studied by
716 Fourier-transform infrared spectroscopy, Biochem. J., 385 (2005) 511-517.
717 [117] A. Barth and C. Zscherp, What vibrations tell us about proteins, Q. Rev. Biophys., 35
718 (2002) 369-430.
719 [118] A.C. Dong, J.D. Meyer, B.S. Kendrick, M.C. Manning and J.F. Carpenter, Effect of
720 secondary structure on the activity of enzymes suspended in organic solvents, Arch. Biochem.
721 Biophys., 334 (1996) 406-414.
722 [119] A.C. Dong, S.J. Prestrelski, S.D. Allison and J.F. Carpenter, Infrared Spectroscopic
723 Studies of Lyophilization-Induced and Temperature-Induced Protein Aggregation, J. Pharm. Sci.,
724 84 (1995) 415-424.
725 [120] M. van de Weert, P.I. Haris, W.E. Hennink and D.J.A. Crommelin, Fourier transform
726 infrared spectrometric analysis of protein conformation: Effect of sampling method and stress
727 factors, Anal. Biochem., 297 (2001) 160-169.
728 [121] M.L. Foresti, G. Valle, R. Bonetto, M.L. Ferreira and L.E. Briand, FTIR, SEM and fractal
729 dimension characterization of lipase B from Candida antarctica immobilized onto titania at
730 selected conditions, Appl. Surf. Sci., 256 1624-1635.
731 [122] J.C. Cruz, P.H. Pfromm, J.M. Tomich and M.E. Rezac, Conformational Changes and
732 Catalytic Competency of Hydrolases Adsorbing on Fumed Silica Nanoparticles: I. Tertiary
733 Structure, Colloids Surf., B, In Press, Accepted Manuscript.
734 [123] A.A. Vertegel, R.W. Siegel and J.S. Dordick, Silica nanoparticle size influences the
735 structure and enzymatic activity of adsorbed lysozyme, Langmuir, 20 (2004) 6800-6807.

[124] M. Rabe, D. Verdes and S. Seeger, Surface-induced spreading phenomenon of protein clusters, Soft matter, 5 (2009) 1039-1047.
[125] L.D. Unsworth, J. van der Oost and S. Koutsopoulos, Hyperthermophilic enzymes - stability, activity and implementation strategies for high temperature applications, FEBS J., 274 (2007) 4044-4056.
[126] M.C. Manning, D.K. Chou, B.M. Murphy, R.W. Payne and D.S. Katayama, Stability of Protein Pharmaceuticals: An Update, Pharm. Res., 27 (2010) 544-575.
[127] H.R. Costantino, R. Langer and A.M. Klibanov, Solid-Phase Aggregation of Proteins under Pharmaceutically Relevant Conditions, J. Pharm. Sci., 83 (1994) 1662-1669.
[128] H.R. Costantino, K.G. Carrasquillo, R.A. Cordero, M. Mumenthaler, C.C. Hsu and K. Griebenow, Effect of excipients on the stability and structure of lyophilized recombinant human growth hormone, J. Pharm. Sci., 87 (1998) 1412-1420.
[129] W.F. Weiss, T.M. Young and C.J. Roberts, Principles, Approaches, and Challenges for Predicting Protein Aggregation Rates and Shelf Life, J. Pharm. Sci., 98 (2009) 1246-1277.

Tables

Table 1

Summary of the amounts of fumed silica and enzyme employed to form the suspensions with different nominal surface coverages. The protein concentration for each suspension was varied from 0.5 mg/mL to 4.70 mg/mL.

		Mass fumed silica (g)					
Enzyme	**Enzyme mass (mg)**	2%SC*	17%SC	100%SC	230%SC	400%SC	1250%SC
CALB	7	0.718	0.092	0.016	0.0068	0.0039	0.0013
TLL	5	0.350	0.040	0.010	0.0030	0.0018	0.0006
s. Carlsberg	5	0.315	0.036	0.009	0.0027	0.0016	0.0005

* The Nominal Surface Coverage (% SC) was calculated as follows:

$$\%SC = \frac{Projected\ area\ of\ enzyme\ molecule}{Nominal\ surface\ area\ of\ Fumed\ Silica} * 100 \qquad \text{Equation 3}$$

The projected area of enzyme is calculated assuming a spherical shape for the enzyme molecules. The diameter of the enzyme molecules from crystallographic data were 6.4 nm [28], 5.0 nm [58], and 4.2 nm [29] for CALB, TLL and *s. Carlsberg*, respectively. The nominal surface area of fumed silica is as provided by the manufacturer: $255 m^2/g$.

Table 2

Band assignments for proteins in the infrared amide I region of the spectrum [121]

Wavenumber [cm^{-1}]	Assignment
1620-1628	Intermolecular β aggregates
1629-1632	β-sheet
1636-1640	β-sheet, antiparallel β-sheet
1645-1657	Disordered
1648-1652	α-helix
1655-1658	α-helix
1668-1674	Turns
1681-1683	Turns
1684-1696	β-sheet

767 Table 3

768 Band assignments for CALB in the infrared amide I region of the spectrum [121]

Wavenumber [cm^{-1}]	Assignment
1622±3	Intermolecular β aggregates
1627±3	β-sheet
1636±3	β-sheet, antiparallel β-sheet
1643±3	Disordered
1660±3	α-helix
1677±3	Turns
1690±3	β-sheet

769

Figure Captions

Fig. 1 CD spectra for native enzymes in aqueous buffer at an enzyme concentration of 0.7 mg/mL. CALB (●), *s. Carlsberg* (○), TLL (▼). The signal at 222 nm can be used as baseline to estimate the α-helical content in the presence of denaturants. Similar plots were obtained for enzyme solutions with other concentrations.

Fig. 2. Chemically-induced unfolding of enzymes. **Equation 1** was employed to compute the unfolded fraction based on signal loss at 222 nm. The unfolding pathways in the presence of denaturants are similar to those reported previously based on intrinsic fluorescence spectroscopy. The relatively modest unfolding for *s. Carlsberg* and TLL after an initial unfolding can be attributed to their high conformational stabilities.

Fig. 3. Unfolding data for CALB on fumed silica (*z*-axis) as a function of initial enzyme concentration (*y*-axis) and nominal surface coverage (*x*-axis). These data will be shown in 3D contour plots to identify regions of conformational stability and to subsequently correlate them with surface loading regimes previously postulated for the lyophilized adsorbates. This approach was introduced in the first part of this series for tertiary unfolding data [122].

Fig. 4. CD spectra for CALB adsorbing on fumed silica nanoparticles at different %SC and at initial enzyme concentrations of: (A) 0.7 mg/mL and (B) 3.3 mg/mL. (Δ) Native, (●) 2%SC, (○) 100%SC, (▼) 400%SC. The signal loss at 222 nm is higher at low %SC for both low and high enzyme concentrations. This was attributed to reduced α-helical content. These results support the notion that increased surface interactions may lead to substantial conformational changes.

Fig. 5. Regions of secondary conformational stability for CALB/Fumed Silica adsorbates. The dotted vertical line at ~250%SC separates two different regions of conformational stability: **Region I** delimited by a long-dash-dot line where adsorbates exhibit low conformational stability, and **Region III** delimited by a short-dash-dot line where highly stable enzyme ensembles are adsorbed on the surface. The presence of these two regions is likely to be responsible for the observed catalytic activity ($\mathbf{r_0}$) of the lyophilized adsorbates in hexane (inset). The poor catalytic competency observed at low %SC can be linked to **Region I** while low activities at high %SC are linked to **Region III** where catalysis is severely reduced by mass transfer limitations. The maximum in activity between those two regions can be attributed to an optimal arrangement on the surface where the structure is relatively well maintained without excessive clustering (**Region II**, delimited by a dotted line). A very similar conformational diagram was previously found from intrinsic fluorescence spectroscopy experiments.

Fig. 6. Secondary unfolding of (A) CALB and (B) *s. Carlsberg* adsorbing on fumed silica nanoparticles in the presence of 30% (v/v) TFE and 0.5 mg/mL DTT. Unfolding with respect to the untreated enzyme was calculated according to $\Delta\phi_{FS} = \phi_{FS \text{ in the presence of TFE or DTT}} - \phi_{FS \text{ for untreated enzyme}}$. The unfolded fractions (ϕ_{FS}) were calculated according to **Equation 2**.

Fig. 7. FTIR spectra in the amide I and II regions of native lyophilized CALB (□) and lyophilized CALB/Fumed silica adsorbates: (▫▫) 2%SC, (∗) 100%SC, (○) 150%SC, (Δ) 230%SC, (▪▪) 300%SC, and (◊) 1250%SC. A clear progression in the surface loading is evidenced by the higher signal intensities as the surface coverage increases.

Fig. 8. Second derivative of the amide I-FTIR spectra of CALB/Fumed silica lyophilized adsorbates. (A) 1250%SC and (B) 2%SC. The secondary structural components associated with the resolution-enhanced bands obtained are subsequently identified according to **Table 3**.

Fig. 9. FTIR spectra and second derivative in the amide I and II regions of lyophilized CALB/Fumed silica adsorbates with 17%SC. Lyophilized nanobiocatalysts were prepared from enzyme solutions with initial concentrations of (A) 0.3 mg/mL and (B) 4.7 mg/mL. The secondary structural components associated with the resolution-enhanced bands are subsequently identified according to **Table 3**.

Supporting Information

Conformational Changes and Catalytic Competency of Hydrolases Adsorbing on Fumed Silica Nanoparticles: II. Secondary Structure

Juan C. Cruz[1], Peter H. Pfromm[1]*, John M. Tomich[2], Mary E. Rezac[1]

(1) Department of Chemical Engineering, Kansas State University, 1005 Durland Hall, Manhattan, KS 66506 - 5106, USA.

(2) Department of Biochemistry and Biotechnology/Proteomics Core Facility, Kansas State University, Burt Hall, Manhattan, KS 66506 - 5106, USA.

Fig. S1. CD spectra for *s. Carlsberg* adsorbing on fumed silica nanoparticles at different %SC and at initial enzyme concentrations of: (A) 0.7 mg/mL and (B) 3.3 mg/mL. (Δ) Native, (●) 2%SC, (○) 100%SC, (▼) 400%SC. As for CALB, the signal loss at 222 nm is higher at low %SC for the two concentrations under consideration. This was attributed to a reduction in the α-helical content due to conformational changes upon contact with the surface.

Fig. S2. CD spectra for TLL adsorbing on fumed silica nanoparticles at different %SC and at initial enzyme concentrations of: (A) 0.7 mg/mL and (B) 3.30 mg/mL. (Δ) Native, (●) 2%SC, (○) 100%SC, (▼) 400%SC. At low enzyme concentration, there is an observable loss of signal at 222 nm for 2%SC and 100%SC. When the enzyme concentration is increased, there is no significant loss of signal for 100%SC and 400%SC. This is most likely due to TLL's conformationally stable structure.

Fig. S3. Regions of secondary conformational stability for *s. Carlsberg*/Fumed Silica adsorbates. The dotted vertical line at ~250%SC separates two different regions of conformational stability. **Region I and III** of low and high conformational stability, respectively. In this case, the catalytic activity ($\mathbf{r_0}$) of the lyophilized adsorbates in hexane (inset) is constantly increasing. It appears that the extent of unfolding while operating in the lower part of **Region I** is less than that observed for CALB in the same region. This resilience to denaturation could be seen as a plausible explanation for the higher activities in this regime of surface loading compared with CALB.

Fig. 1

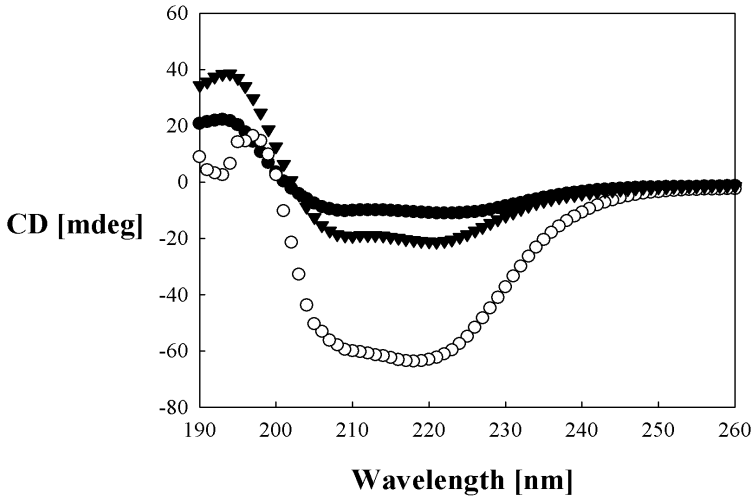
60
40
20
0
-20
-40
-60
-80
CD [mdeg]
190
200
210
220
230
240
250
260
Wavelength [nm]

Fig. 2

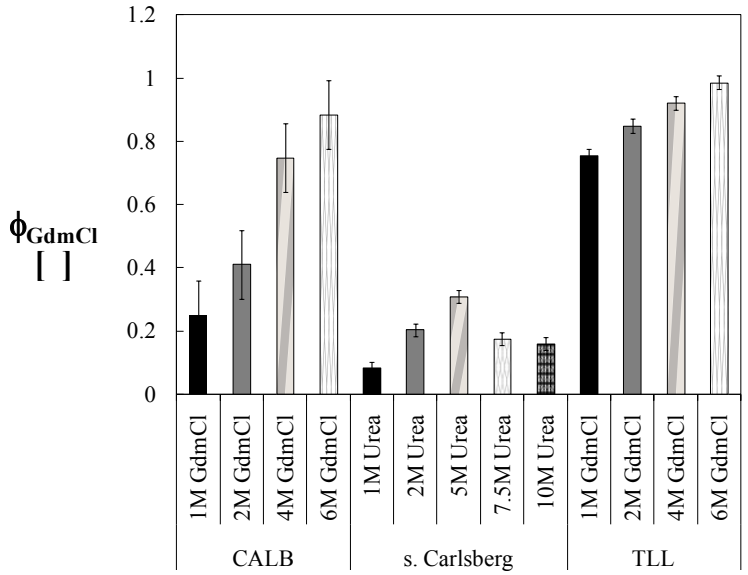
ϕ_{GdmCl} [ ]
1.2
1
0.8
0.6
0.4
0.2
0
1M GdmCl
2M GdmCl
4M GdmCl
6M GdmCl
1M Urea
2M Urea
5M Urea
7.5M Urea
10M Urea
1M GdmCl
2M GdmCl
4M GdmCl
6M GdmCl
CALB
s. Carlsberg
TLL

Fig. 3

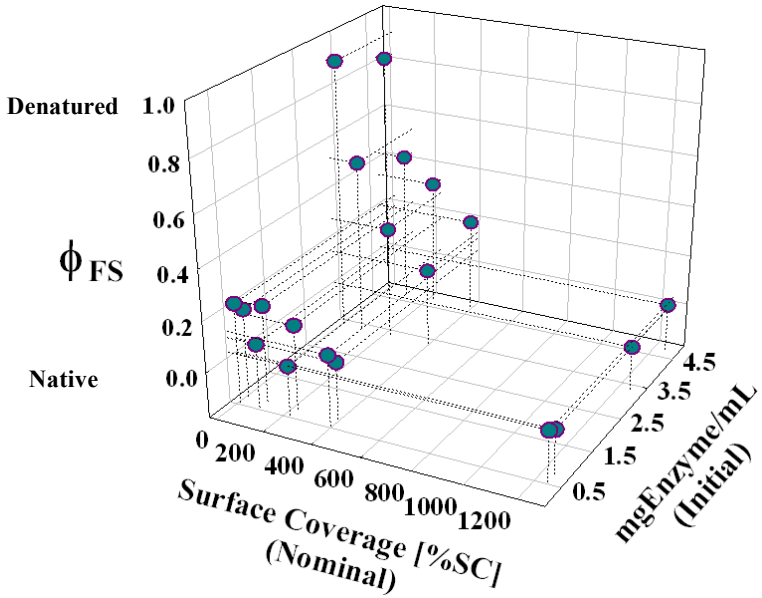
Denatured
1.0
0.8
0.6
ϕ FS
0.4
0.2
Native
0.0
0
200
400
600
800
1000
1200
Surface Coverage [%SC]
(Nominal)
0.5
1.5
2.5
3.5
4.5
mgEnzyme/mL
(Initial)

Fig. 4

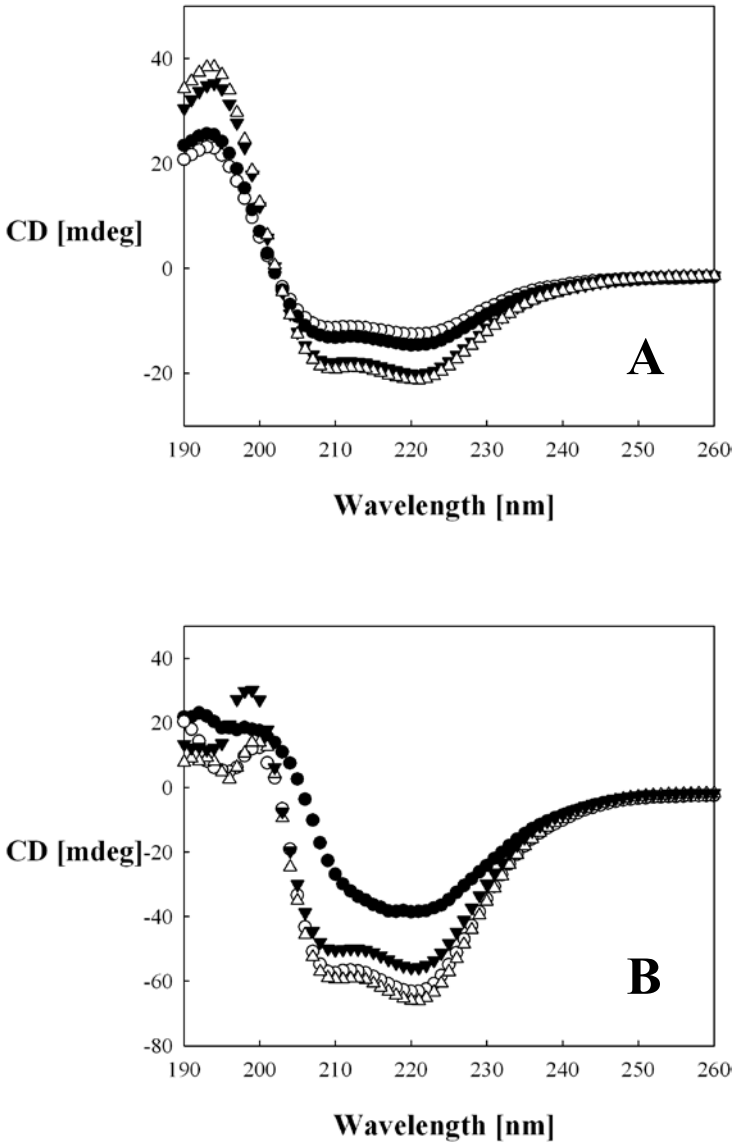
CD [mdeg]
40
20
0
-20
190
200
210
220
230
240
250
260
Wavelength [nm]
A
CD [mdeg]
40
20
0
-20
-40
-60
-80
190
200
210
220
230
240
250
260
Wavelength [nm]
B

Fig. 5

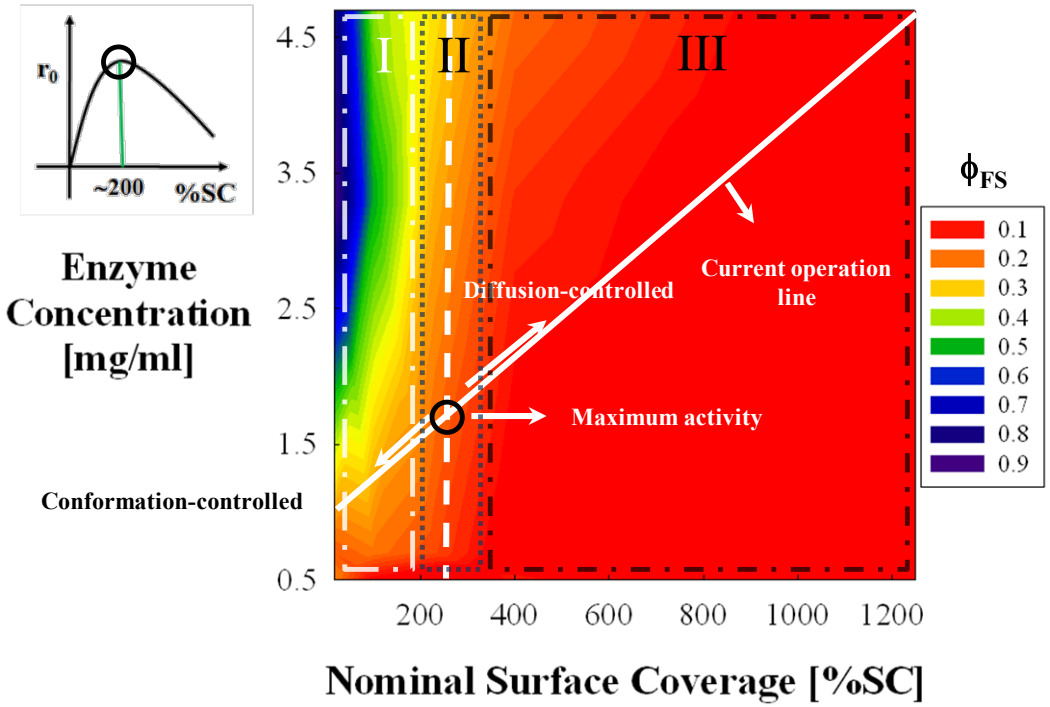
r0
~200
%SC
Enzyme Concentration [mg/ml]
4.5
3.5
2.5
1.5
0.5
I
II
III
Diffusion-controlled
Current operation line
Maximum activity
Conformation-controlled
ϕFS
0.1
0.2
0.3
0.4
0.5
0.6
0.7
0.8
0.9
200
400
600
800
1000
1200
Nominal Surface Coverage [%SC]

Fig. 6

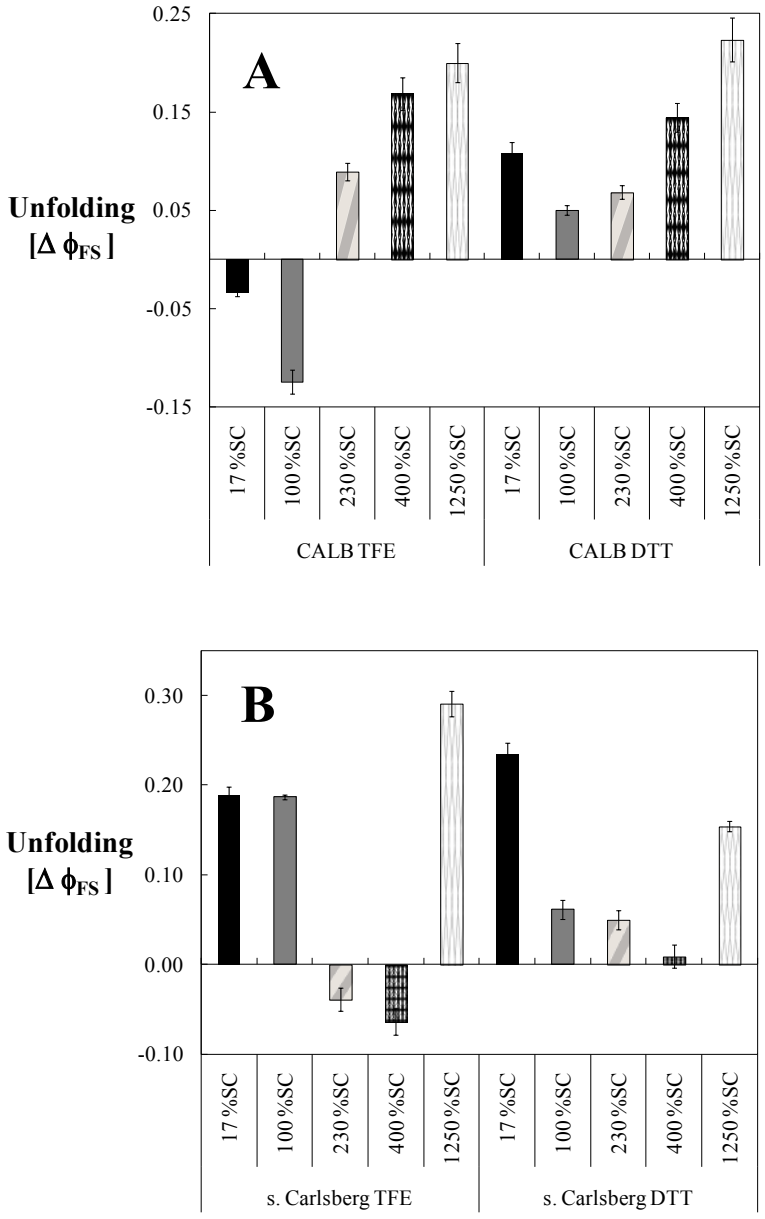
A
Unfolding
[Δ ϕFS]
0.25
0.15
0.05
-0.05
-0.15
17 %SC
100 %SC
230 %SC
400 %SC
1250 %SC
17 %SC
100 %SC
230 %SC
400 %SC
1250 %SC
CALB TFE
CALB DTT
B
Unfolding
[Δ ϕFS]
0.30
0.20
0.10
0.00
-0.10
17 %SC
100 %SC
230 %SC
400 %SC
1250 %SC
17 %SC
100 %SC
230 %SC
400 %SC
1250 %SC
s. Carlsberg TFE
s. Carlsberg DTT

Fig. 7

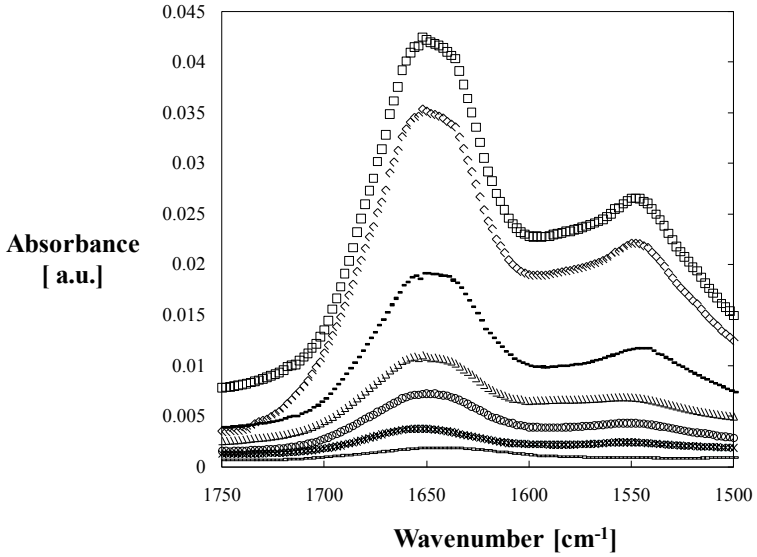
0.045
0.04
0.035
0.03
0.025
0.02
0.015
0.01
0.005
0
Absorbance
[a.u.]
1750
1700
1650
1600
1550
1500
Wavenumber [cm-1]

Fig. 8

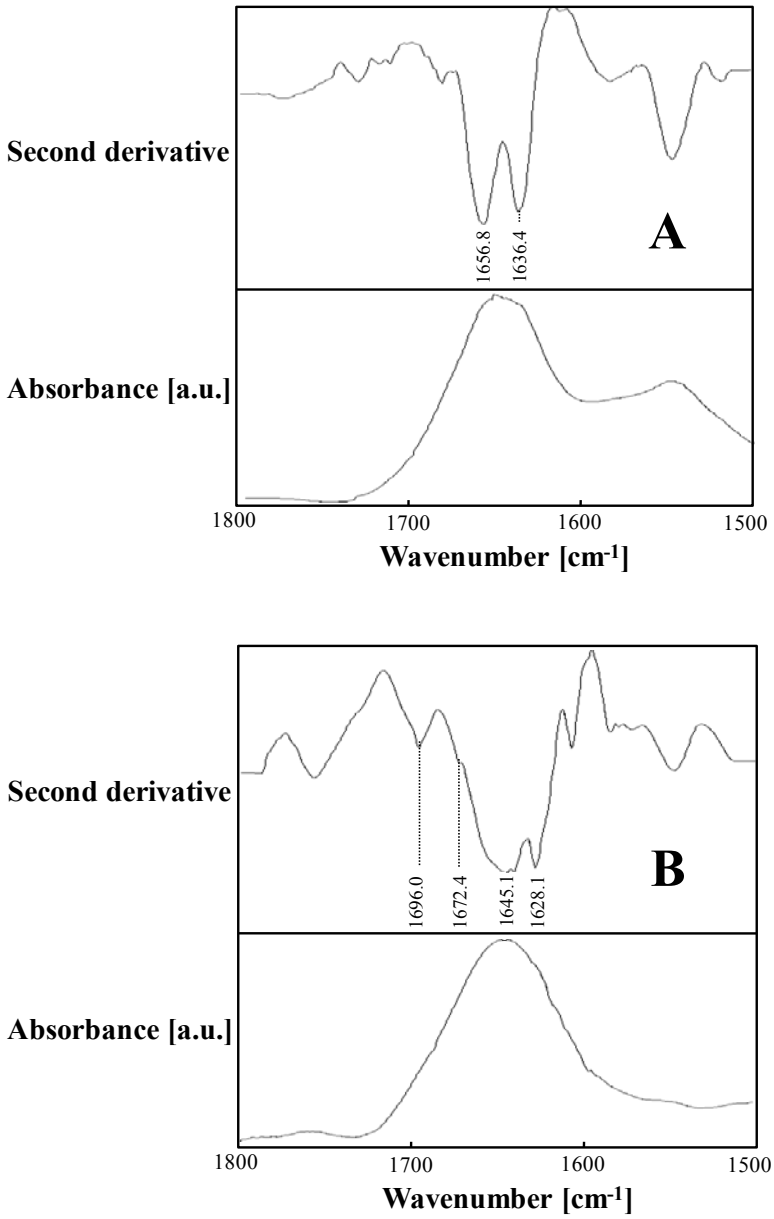
Second derivative
1656.8
1636.4
A
Absorbance [a.u.]
1800
1700
1600
1500
Wavenumber [cm-1]
Second derivative
1696.0
1672.4
1645.1
1628.1
B
Absorbance [a.u.]
1800
1700
1600
1500
Wavenumber [cm-1]

Fig. 9

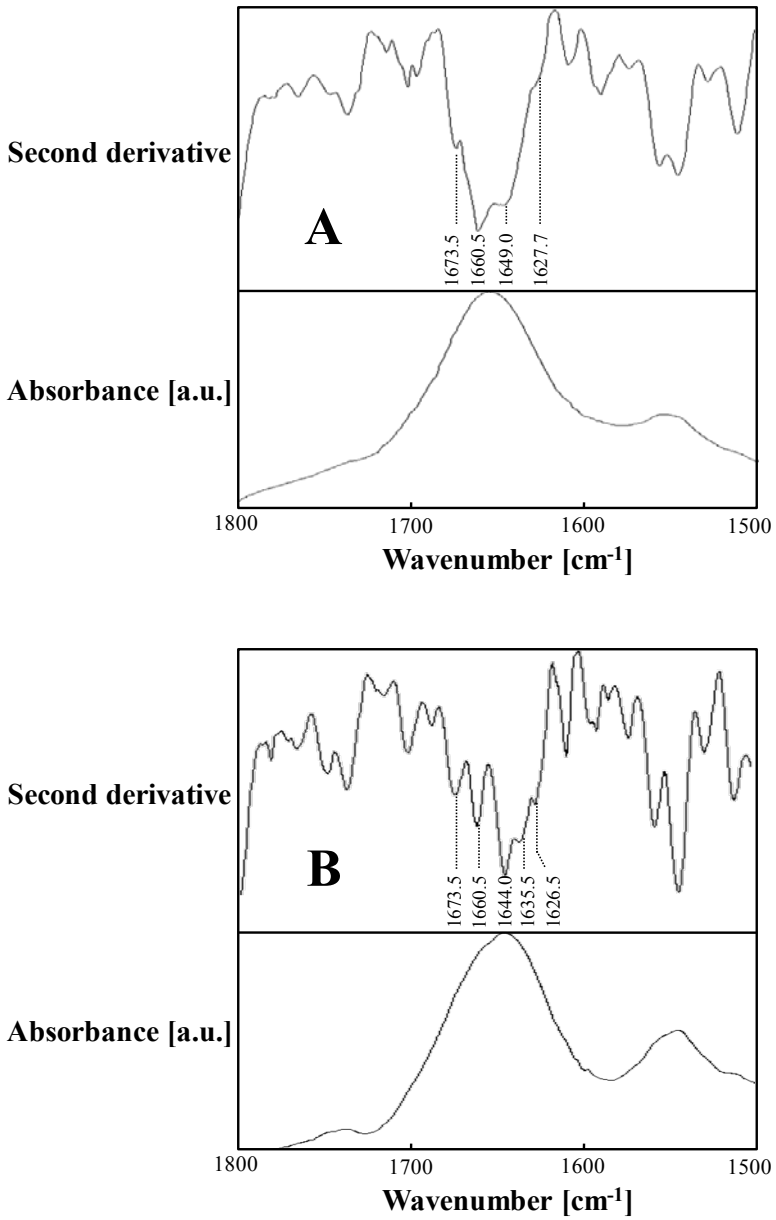
Second derivative
A
1673.5
1660.5
1649.0
1627.7
Absorbance [a.u.]
1800
1700
1600
1500
Wavenumber [cm-1]
Second derivative
B
1673.5
1660.5
1644.0
1635.5
1626.5
Absorbance [a.u.]
1800
1700
1600
1500
Wavenumber [cm-1]

Fig. S1

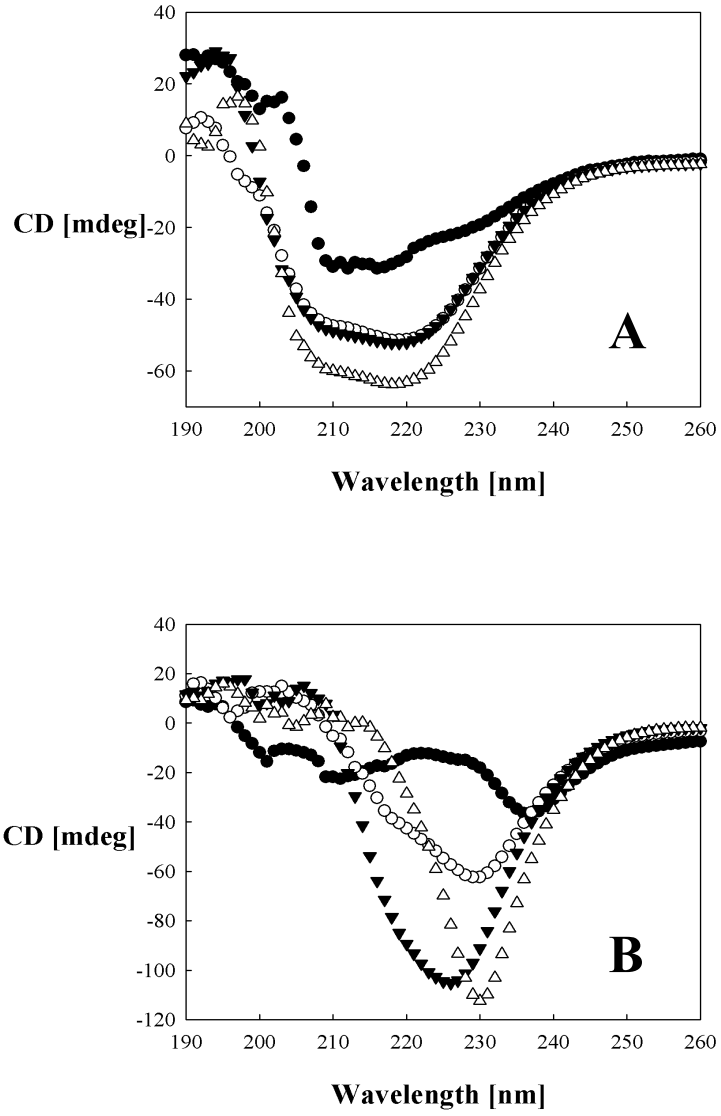
40
20
0
-20
-40
-60
CD [mdeg]
A
190
200
210
220
230
240
250
260
Wavelength [nm]
40
20
0
-20
-40
-60
-80
-100
-120
CD [mdeg]
B
190
200
210
220
230
240
250
260
Wavelength [nm]

Fig. S2

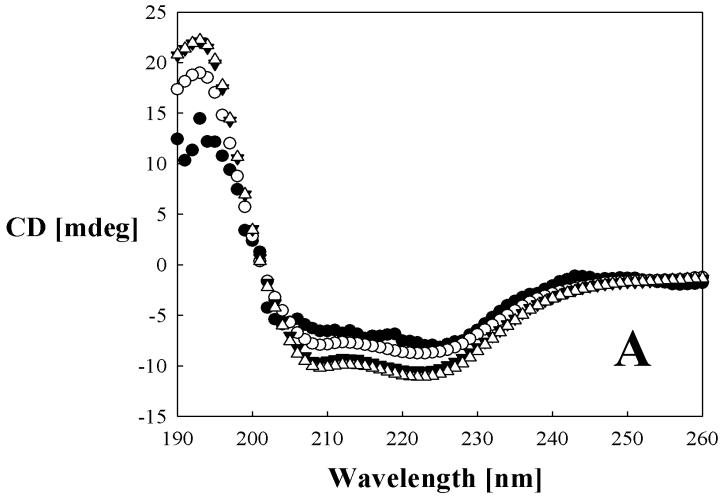
CD [mdeg]
25
20
15
10
5
0
-5
-10
-15
190
200
210
220
230
240
250
260
Wavelength [nm]
A

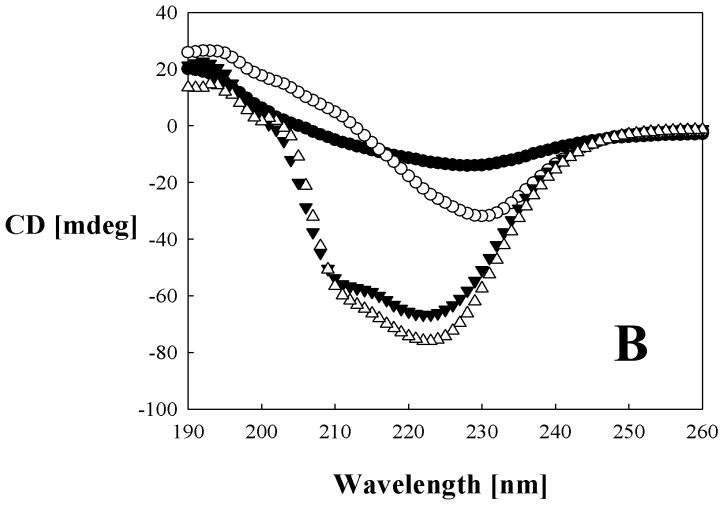
CD [mdeg]
40
20
0
-20
-40
-60
-80
-100
190
200
210
220
230
240
250
260
Wavelength [nm]
B

Fig. S3

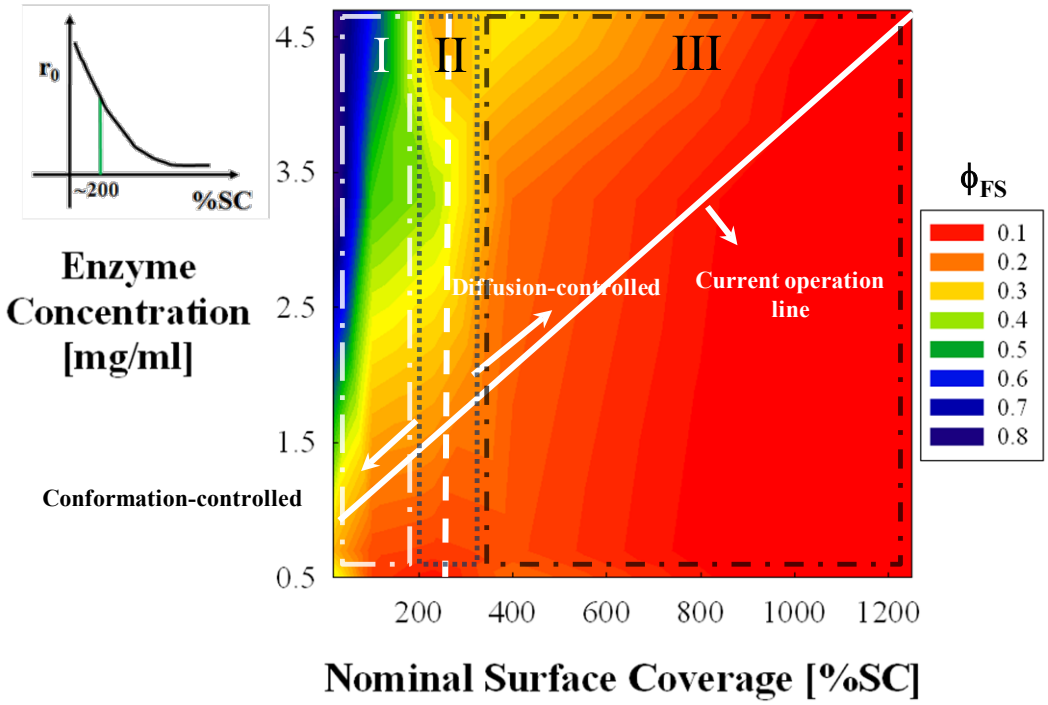
r0
~200
%SC
Enzyme Concentration [mg/ml]
4.5
3.5
2.5
1.5
0.5
I
II
III
Diffusion-controlled
Current operation line
Conformation-controlled
ϕFS
0.1
0.2
0.3
0.4
0.5
0.6
0.7
0.8
200
400
600
800
1000
1200
Nominal Surface Coverage [%SC]